Effects of Different Compatibilizers on the Rheological, Thermomechanical, and Morphological Properties of HDPE/LLDPE Blend-Based Nanocomposites

Fabio Roberto Passador, Adhemar Collà Ruvolo-Filho, Luiz Antonio Pessan

Federal University of São Carlos, Department of Materials Engineering, Rodovia Washington Luís, Km 235, P.O. Box 676, São Carlos, SP, 13565-905, Brazil

Correspondence to: L. A. Pessan (E-mail: pessan@ufscar.br)

ABSTRACT: The influence of two different compatibilizers and their combination (maleic anhydride grafted high density polyethylene, HDPE-g-MA; maleic anhydride grafted linear low density polyethylene, LLDPE-g-MA; and 50/50 wt % mixture of these compatibilizers) on the rheological, thermomechanical, and morphological properties of HDPE/LLDPE/organoclay blend-based nanocomposites was evaluated. Nanocomposites were obtained by melt-intercalation in a torque rheometer in two steps. Masterbatches (compatibilizer/nanoclay 2:1) were obtained and subsequently diluted in the HDPE/LLDPE matrix producing nanocomposites with 2.5 wt % of nanoclay. Wide angle X-ray diffraction (WAXD), steady-state rheological properties, and transmission electron microscopy (TEM) were used to determine the influence of different compatibilizer systems on intercalation and/or exfoliation process which occurs preferentially in the amorphous phase, and thermomechanical properties. The LLDPE-g-MA with a high melt index (and consequently low viscosity and crystallinity) was an effective compatibilizer for this system. Furthermore, the compatibilized nanocomposites with LLDPE-g-MA or mixture of HDPE-g-MA and LLDPE-g-MA exhibited better nanoclay's dispersion and distribution with stronger interactions between the matrix and the nanoclay. These results indicated that the addition of maleic anhydride grafted polyethylene facilitates both, the exfoliation and/or intercalation of the clays and its adhesion to HDPE/LLDPE blend. © 2013 Wiley Periodicals, Inc. J. Appl. Polym. Sci. 000: 000–000, 2013

INTRODUCTION

Polymer blends composed of high-density polyethylene (HDPE) and linear low density polyethylene (LLDPE) has attracted considerable interest both in the research community and in industry.[1,2] As a widely used polyolefin, HDPE possesses excellent chemical resistance, tensile properties, and hardness. However, usually HDPE material with high mechanical properties required for some applications has very low melt flow index and more difficult processability. This problem can be overcome through the addition of another component more easily processable into HDPE. Evidently, good compatibility between these two components is also required and the LLDPE is a suitable candidate for such purpose. The advantages of the HDPE/LLDPE blends include, for example, improvements in impact strength, optical properties, low temperature impact strength, rheological properties, and overall mechanical behavior.[3–5] Interest in polyolefin nanocomposites has emerged due to their improved performance in packing and engineering applications.

Because of the light weight, good process ability, low cost, etc. polyethylene is the most common polymers which used as a matrix.[6–9]

In recent years, polymer/clay nanocomposites have generated great interests in the polymer industry as a type of composite material because of their superior properties such as high heat deflection temperature, gas barrier performance, dimensional stability, enhanced mechanical properties, optical clarity, and flame retardancy when compared with the pure polymer or composites having conventional fillers.[10] Recently, three ways are used to prepare polymer/clay nanocomposites: the solution method, *in situ* polymerization and melt intercalation method. Depending on the interfacial interactions between the polymer chains and clay layers, the final structure of a polymer/clay nanocomposite could be exfoliated (separation of platelets from one another and dispersed individually in the polymer matrix) or intercalated (polymer is inserted between the layers of the clay such that the interlayer spacing is expanded, but the

Table I. Composition of the Samples Prepared

Samples	HDPE	LLDPE	Blend	Nano1	Nano2	Nano3	Nano4
HDPE	100		75	73	69.5	69.5	69.5
LLDPE		100	25	24.5	23	23	23
HDPE-g-MA					5		2.5
LLDPE-g-MA						5	2.5
Cloisite 20A				2.5	2.5	2.5	2.5

layers still bear a well-defined spatial relationship to each other).[10–12]

Clays can be efficiently exfoliated in polar polymers when the correct processing conditions are used[13,14]; however, it is very difficult to obtain a well-exfoliated nanocomposite structure for non-polar polymers like polyethylene because polyolefins are hydrophobic and lack suitable interactions with the polar aluminosilicate surface of the clay.[15–18] The strategy to improve interfacial interactions between the clay and the non-polar matrix is the chemical modification of these resins, in particular, the grafting of pendant anhydride groups, which has been used successfully to overcome problems associated with poor phase adhesion in polyolefin/clay nanocomposites and increases the polarity and improves exfoliation in polyethylene.[19,20]

Several polymer systems based on polyethylene–clay nanocomposites have been studied lately.[21–23] Hotta and Paul[24] studied LLDPE–clay nanocomposites prepared by melt compounding using a maleic anhydride-grafted linear low density polyethylene (LLDPE-g-MA) as a compatibilizer and showed that LLDPE-g-MA is an effective compatibilizer for this system once the organoclay was well-exfoliated in the matrix with improve mechanical properties suggesting that the LLDPE-g-MA may promote adhesion of the LLDPE molecules to the clay particles. Gopakumar et al.[25] investigated the use of high density polyethylene-grafted maleic anhydride (HDPE-g-MA) as compatibilizer in HDPE–clay nanocomposites and showed that to obtain a structure consisting of partially exfoliated and/or intercalated clay it is necessary to chemically modify both polyolefin and montmorillonite. Furthermore, the authors showed that the nanoscale dispersed clay layers act as nucleating agents, resulting in enhanced polymer crystallization rate, increased crystallization temperature, and reduced degree of crystallinity. Ryu and Chang,[26] in turn, studied LLDPE–clay nanocomposites prepared by melt compounding using HDPE-g-MA as a compatibilizer. The authors observed that the degree of exfoliation of montmorillonite is strongly dependent on the concentration of HDPE-g-MA and on the concentration of grafted maleic anhydride in HDPE-g-MA.

From these studies, it is evident that both HDPE-g-MA and LLDPE-g-MA can be used as compatibilizing agents between polyethylenes and nanoclays. Thus, this study investigates the effects of different compatibilizer systems (HDPE-g-MA, LLDPE-g-MA, and 50/50 wt % mixture of these compatibilizers) on the clay dispersion state of HDPE/LLDPE blend-based

nanocomposites. Another goal was to characterize the influence of these compatibilizer systems on the rheological, thermomechanical, and crystallization properties of polyethylene.

EXPERIMENTAL

Materials

The HDPE DMDA 6200 NT-7 with a melt index of 0.38 g/10 min (190°C/2.16 kg) was supplied by Dow Chemical. The LLDPE with a melt index of 29 g/10 min (190°C/2.16 kg) commercially designated as IC 32, was supplied by Braskem (Brazil). The high density polyethylene-grafted maleic anhydride (HDPE-g-MA), with 1 wt % maleic anhydride and a melt index of 3.5 g/10 min (190°C/2.16 kg) and the linear low density polyethylene-grafted maleic anhydride (LLDPE-g-MA), with 1 wt % maleic anhydride and a melt index of 30 g/10 min (190°C/2.16 kg), supplied by Crompton Corporation were used as compatibilizers. The LLDPE and LLDPE-g-MA were chosen because they have the same melt index and it is expected that they are miscible with each other based on related works in the literature.[27,28] The HDPE and HDPE-g-MA were also chosen based on their melt indexes. Thus, it is expected that the compatibilizers and the polymers employed are miscible with each other, and the HDPE/LLDPE compatibilized blend have better affinity with organic modifier of the organoclay.

Organophilic montmorillonite (20A; Cloisite® 20A) used in this study was purchased from Southern Clay. The organoclay 20A is ion-exchanged with dimethyl dehydrogenated tallow ammonium ions, where tallow is composed predominantly of octadecyl chains with smaller amount of lower homologues. This organoclay was selected based upon recent studies showing improved organoclay exfoliation in polyethylene using surfactants with two tails on the ammonium ion instead of one tail.[19,23,29] It was found that organoclay 20A contains organic modifier of about 38 wt % by TGA measurement.

Preparation of the Composite Systems by Melt Processing

All materials were dried for a minimum of 24 h in a vacuum oven at 80°C prior to melt processing. In order to study the influence of the addition of different compatibilizer agent on the morphology and rheological properties of the HDPE/LLDPE blend based nanocomposites, three compatibilizer systems (HDPE-g-MA, LLDPE-g-MA, and 50/50 wt % mixture of these compatibilizers) were studied. The samples were prepared by melt-intercalation in a torque rheometer Haake, model Rheomix 600p, using counter-rotational and interpenetrated rotors, operated at 180°C, 80 rpm for 10 min. The nanocomposites Nano2, Nano3, and Nano4 were prepared in two steps. Masterbatches (MB; compatibilizer/20A 2:1) were obtained in a torque rheometer Haake (180°C, 80 rpm for 10 min) and subsequently diluted in the HDPE/LLDPE matrix. All the nanocomposites had a final concentration of 2.5 wt % of organoclay, and blend ratio 3:1 (HDPE/LLDPE). Table I shows the composition of the systems prepared.

Although the effect of mixing time is very important for compatibilized nanocomposites in the case of non-compatibilized nanocomposite of polyolefins (Nano 1), there is no significant change on interlayer distances as shown in the literature.[6,10,30,31]
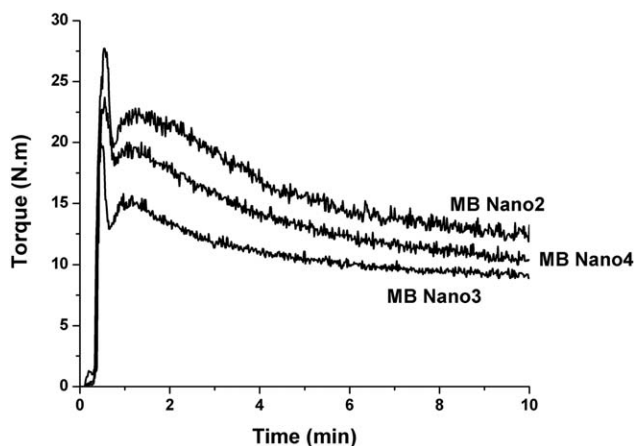
Figure 1. Variation of torque during the masterbatches preparation.

Characterization by Infrared Spectroscopy (FTIR)

HDPE, LLDPE, and their respective nanocomposites were compressed into 50 μm thick films and then analyzed by FTIR measurements using a Perkin Elmer Spectrum 1000 spectrophotometer. The nanoclay and the MB were mixed with KBr and pressed into discs. Each infrared spectrum was the average of 16 scans at the resolution of 4 cm^{-1}.

Determination of Crosslinking Density in the Masterbatches

The crosslinking content of the MB was obtained through swelling measurements. The uncrosslinked HDPE was first removed by a Soxhlet extraction in toluene (100°C) for 7 days and then the swollen samples were dried at 70°C in a vacuum oven for 3 days. The crosslinking content was determined by mass loss of the samples. The organoclay content was subtracted from the equation. For this, the residues of the MB were determined by thermogravimetric analysis (TGA), performed on a Q50 TA Instruments, from room temperature to 800°C at a rate of 2°C/min, under N$_2$ atmosphere. The content of surfactant in the organoclay was also considered in the equation. The crosslinking content was calculated using the follow equation:

$$\% \, \text{crosslinking} = \frac{(\text{total weight after extraction} - \text{weight of nanoclay})}{(\text{initial weight} - \text{weight of nanoclay})} \tag{1}$$

where the weight of nanoclay was obtained by TGA curve of the MB.

Characterization of the Nanocomposites

Wide-Angle X-Ray Diffraction (WAXD). The WAXD measurements were conducted in a Rigaku GE/Gerflex Analix diffractometer, with Cu $K\alpha$ radiation ($\lambda = 1.54056$ Å), operating at 40 kV and 25 mA at a scan rate of 1°/min in a range of 2θ from 1.6 to 30°. The diffraction patterns data were used to calculate the degrees of crystallinity and the crystallite sizes. Subsequently, the peaks in WAXD profiles, were mathematical deconvoluted

by using a Gaussian function and the overall crystallinity X_c was calculated by

$$X_c = \frac{\sum A_{\text{cryst}}}{\sum A_{\text{cryst}} + \sum A_{\text{amorp}}} \tag{2}$$

where A_{cryst} and A_{amorp} are the fitted areas of crystal and amorphous peaks, respectively. The samples used were prepared by compression molding with the thickness of 0.2 mm.

The apparent crystalline size was determined according to Scherrer's equation:

$$D_{(hkl)} = \frac{K\lambda}{\beta \cos \theta} \tag{3}$$

where β is the half-width of the diffraction peak in radians, K is equal to 0.9 considering that the particle have a spherical geometry, θ is the Bragg angle, and $\lambda = 1.54$ Å, is the wavelength of the Cu $K\alpha$ X-rays. The values of $D_{(hkl)}$ for (110) reflection were calculated.

Differential Scanning Calorimetry (DSC). The DSC equipment used was a TA Instruments QS100, under N$_2$ atmosphere. The measurements of neat HDPE, LLDPE, and HDPE/LLDPE (75/25) blend were performed as following procedures: samples were heated to 180°C at 10°C/min and kept for 5 min to erase any previous thermal history, then cooled to 40°C at 10°C/min.

Rheological Properties. To evaluate the state of distribution of the nanoclay in the matrix, the steady-state rheological properties of the nanocomposites were measured in a controlled stress rheometer AR G2 from TA Instruments with geometry of parallel plates, with a plate diameter of 25 mm and gap between plates of 1 mm, under nitrogen atmosphere, at 180°C.
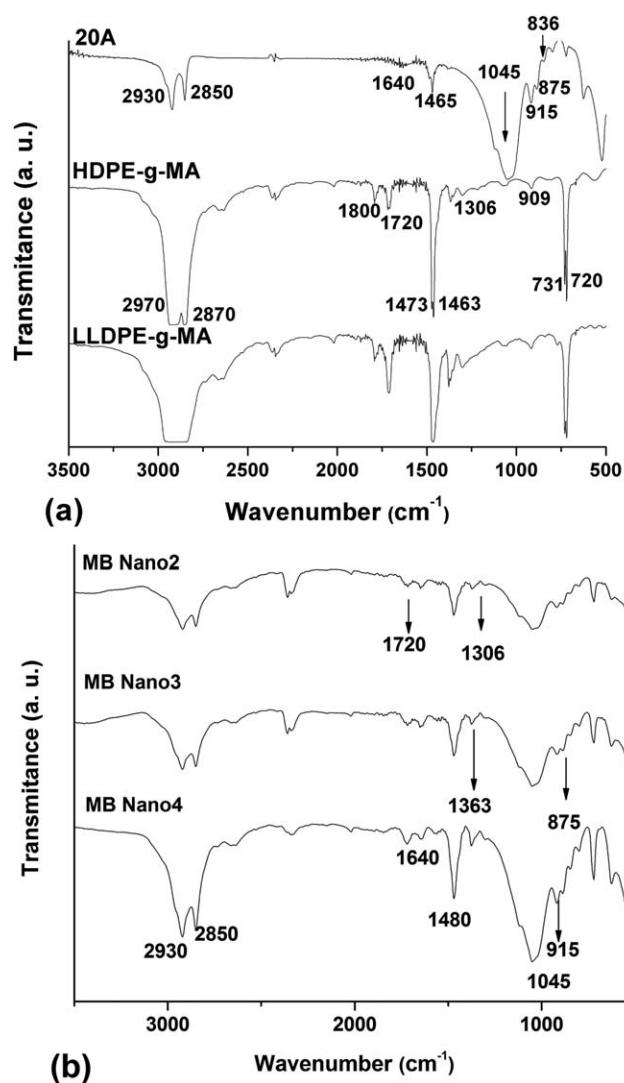
Morphology Characterization. The samples were examined by transmission electron microscopy (TEM). Ultra-thin sections about 45 nm thick were cryogenically cut from the samples. The nanocomposites samples and the diamond knife were cooled between −75 and −85°C and −60°C, respectively, using liquid nitrogen. Cut sections were collected onto 400 mesh grids and dried with filter paper. The sections were analyzed using a Philips CM120 transmission electron microscope at an acceleration voltage of 120 kV.

Thermomechanical Properties. The thermomechanical behavior of the samples was examined using a dynamic mechanical analyze (DMA), performed on a Q800 TA Instruments. The experiments were carried out in bending mode on the specimens from −130 to 110°C at a rate of 2°C/min and at frequency of 1 Hz.

RESULTS AND DISCUSSION

Torque Rheometer Curves and Infrared Spectroscopy Characterization

The torque data collected during the processing of the MB are shown in Figure 1. The first torque peak is related to the compatibilizer agent melting. HDPE-g-MA and LLDPE-g-MA have different melt indexes and viscosities during mixing which caused difference in the equilibrium torque. Moreover, it was

Figure 2. Infrared spectra (a) 20A, HDPE-*g*-MA, and LLDPE-*g*-MA and (b) masterbatches. The curves are vertically offset for clarity.

asymmetric and symmetric vibration methylene groups $(CH_2)n$ of the aliphatic carbon chain. IR peaks at 915, 875, and 836 cm^{-1} are attributed to Al—OH—Al, Al—OH—Fe, and Al—OH—Mg bending vibration, respectively; 1045 cm^{-1} corresponded to the Si—O—Si silicate stretching frequency, the band at 1465 cm^{-1} corresponded to the C—H axial deformation, and the band at 1640 cm^{-1} corresponded to the O—H deformation vibrations of physically adsorbed water molecules. The infrared spectra for the compatibilizers [Figure 2(a)] showed the bands at 2970 and 2870 cm^{-1} that are attributed to the asymmetric and symmetric vibration methylene groups $(CH_2)n$ of the aliphatic carbon chain. IR peaks at 1473 and 1463 cm^{-1} are attributed to C—H angular deformation and the bands at 731 and 720 cm^{-1} corresponded to —CH$_2$ symmetric angular deformation. The 1363 and 1306 cm^{-1} bands corresponded to the —CH$_2$ axial deformation of the compatibilizers. In addition, there is also C=O axial deformation band at 1720 and 1800 cm^{-1} due to the presence of the maleic anhydride. It can be observed in the infrared spectra of the MB [Figure 2(b)] the presence of all bands of 20A and the compatibilizers. The prominent IR bands are shown in Table II.

The crosslink formation between the polyethylene chains during the preparation of the MB could be observed by FTIR through the band at 1640 cm^{-1} which is related to the stretching vibration of the C=C bond, that is a precursor to initiate the crosslinking,[32,33] however, this same band corresponds to the O—H deformation vibrations of physically adsorbed water molecules from the organoclay.

In order to confirm and quantify the crosslinking formation in the MB all the uncrosslinked HDPE was removed by Soxleht extraction in toluene. Figure 3 shows the thermograms obtained during TGA scans for the MB. From TGA curves, it can be clearly observed the weight loss and calculated the residue in the samples. The crosslinking content results are shown in Table III. It was possible to calculate the crosslinking content for the MB prepared and it can be observed that the crosslinking

observed that there is an increase in the torque with mixing time for all compatibilizer systems which could be correlated to the mechanisms involved in the polyethylene degradation through crosslinking and/or an increase in the interactions between the components.

Crosslinks can be occurs due to the increase in temperature during melt processing (viscous heating). During mixing, viscous heat is dissipated due to the friction between the highly viscous polymer melt, the nanoclay, and the metal surfaces of the processing equipment in contact with the polymer mixture. The crosslink formation in the MB during the melt processing was investigated by FTIR. The infrared spectra of the compatibilizers (HDPE-*g*-MA and LLDPE-*g*-MA), 20A, MB produced with HDPE-*g*-MA/20A (MB Nano2), LLDPE-*g*-MA/20A (MB Nano3), and HDPE-*g*-MA/LLDPE-*g*-MA/20A (MB Nano4) are presented in Figure 2.

The infrared spectrum for Cloisite 20A [Figure 2(a)] showed peaks at 2930 and 2850 cm^{-1} that are ascribed to the

Table II. Observed IR Frequencies of the Samples

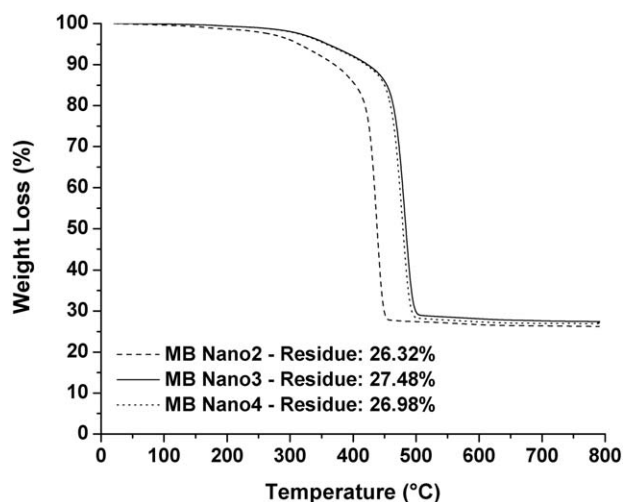| Wavenumber (cm^{-1})	Assignment
2970, 2850	Asymmetric and symmetric vibration of methylene groups $(CH_2)n$
1720	C=O axial deformation
1640	O—H deformation; C=C stretching vibration
1480	C—H angular deformation
1473, 1463	C—H angular deformation
1363, 1306	—CH$_2$ axial deformation
1045	Si—O—Si silicate stretching
915	Al—OH—Al aluminate deformation
909	Terminal vinyl deformation
875	Al—OH—Fe aluminate deformation
836	Al—OH—Mg aluminate deformation
731, 720	—CH$_2$ symmetric angular deformation

Figure 3. TGA analysis of the masterbatches.

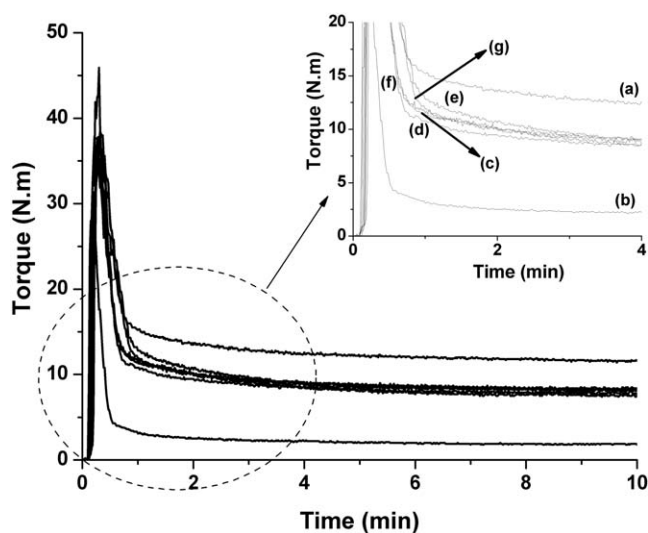**Figure 4.** Variation of torque during mixing of (a) HDPE, (b) LLDPE, (c) HDPE/LLDPE blend, (d) Nano1, (e) Nano2, (f) Nano3, and (g) Nano4.

formation occurs mainly to LLDPE-g-MA phase. The HDPE-g-MA despite presenting a small content of crosslinking (2.1%), the increase in the equilibrium torque observed can be related to increase in the interactions between the components. This fact can be confirmed by comparing the content of crosslinking obtained for the MB with 50/50 wt % mixture of HDPE-g-MA and LLDPE-g-MA.

Figure 4 shows the variation of torque during mixing of the HDPE, LLDPE, HDPE/LLDPE blend, and nanocomposites. The torque peak corresponds to the addition of the compounds. The Nano2, Nano3, and Nano4 compositions were prepared in two steps. Since the shear rate imposed during this processing is the same in all cases, some change in the torque at equilibrium (i.e., melt viscosity) should be expected due the presence of an inorganic filler, compared to the HDPE/LLDPE blend. It was not observed the increase in the torque with mixing time for the nanocomposites.

In order to verify whether crosslinking formation also occurred in the nanocomposites during the melt processing, samples of these nanocomposites were investigated by FTIR. The infrared spectra of the pristine organoclay, HDPE, LLDPE, HDPE/LLDPE blend, and the nanocomposites are presented in Figure 5.

It was observed the same bands in the spectrum of HDPE-g-MA, LLDPE-g-MA, and 20A [Figure 2(a)]. It can be noted, in Figure 5, that the differences in HDPE/LLDPE blend spectrum (curve d) and nanocomposites spectra (curves e, f, g, and h) were due to the organoclay addition. FTIR studies clearly

Table III. Values of Residue and Crosslinking Content of the Masterbatches

Sample	Residue (%)	Crosslinking (%)
MB Nano2	26.32	2.1
MB Nano3	27.48	22.4
MB Nano4	26.98	11.7

indicate the formation of HDPE/LLDPE blend-based nanocomposites however it did not indicate crosslinking formation. Thus, the formation of a small amount of crosslinking observed during the preparation of the MB was not observed in the preparation of the nanocomposites during its processing.

However, the crosslinking formation can affect the increase of the organoclay interlayer spacing. The intercalation and/or exfoliation process occurs as a result of the diffusion of the compatibilizer polymer matrix molecules to the interlamellar spaces of the organoclay. If the polyethylene chains, with a low level of crosslinking diffuse into the interlamellar space this polymer molecule with higher molecular weight can lead to a more
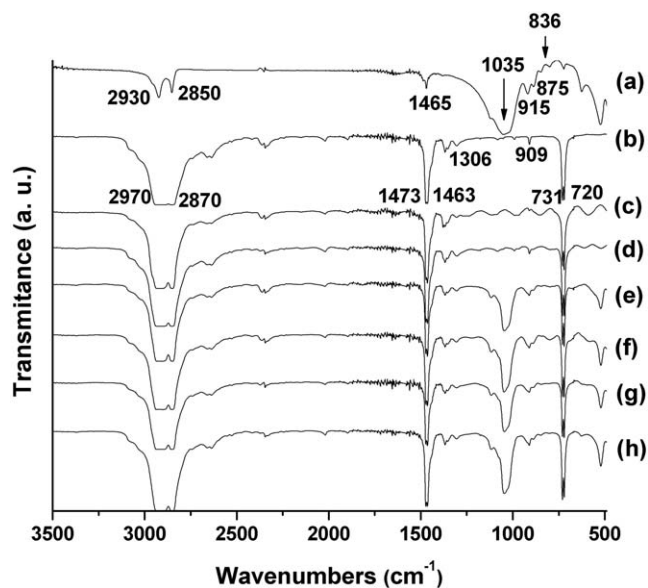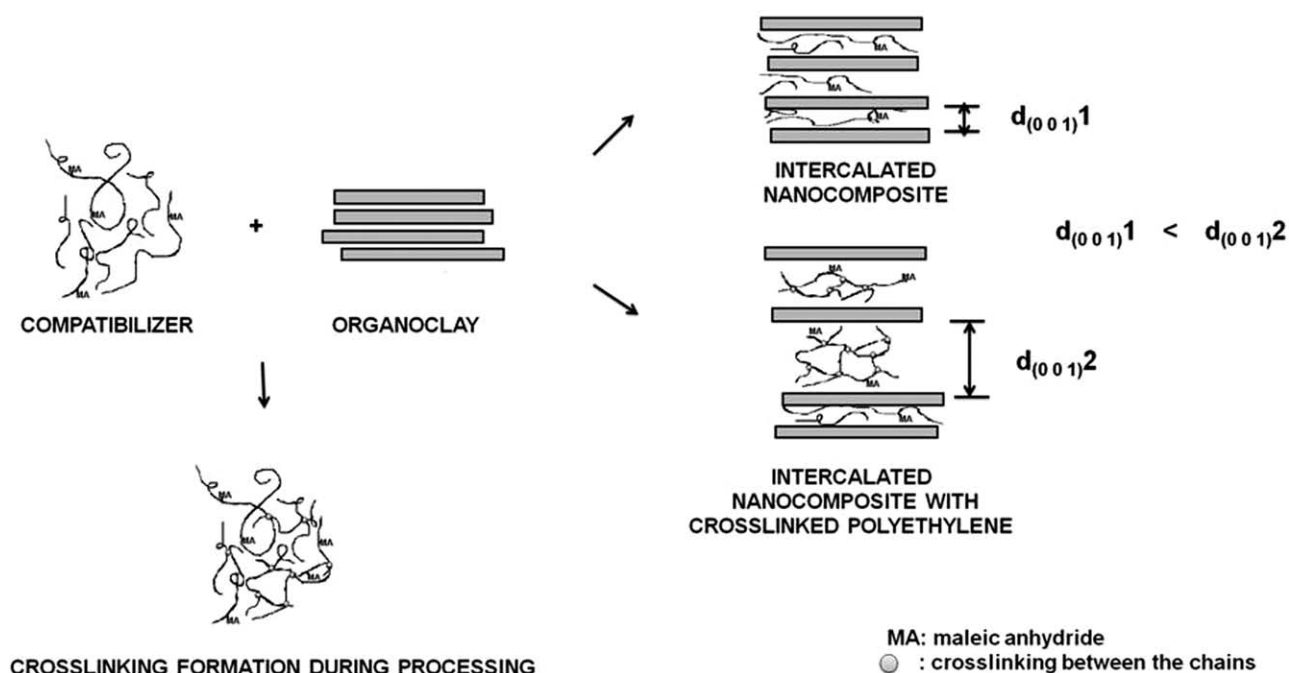

Figure 5. Infrared spectra of (a) 20A, (b) HDPE, (c) LLDPE, (d) HDPE/LLDPE blend, (e) Nano1, (f) Nano2, (g) Nano3, and (h) Nano4. The curves are vertically offset for clarity.

Figure 6. Representation of the increase in the interlayer distance with the diffusion of the crosslinked polyethylene.

significant increase in the interlayer distance when compared to a similar molecule without crosslinking. A scheme for the increase of interlayer distance with the diffusion of crosslinked polyethylene is suggested in Figure 6.

The diffusion of crosslinked polyethylene chains from the MB previously prepared is facilitated because the molecule has polar groups (due to the maleic anhydride) which increase the interaction with the surfactant of the organoclay. The addition of crosslinked polyethylene molecules can increase the interlayer distance, however, the increase in molecular weight due this process can hinder the diffusion of the crosslinked polyethylene chains into the interlayer clay gallery. Therefore, for this process to occur there should be a critical chain size, with a critical molar mass, with addition of polar groups, and adequate positioning of the polar groups along the molecule that can facilitate the diffusion of crosslinked chains into the interlayer organoclay galleries.

WAXD and DSC Analysis
The WAXD patterns of neat organoclay (20A) and the nanocomposites prepared from different compatibilizer systems are shown in Figure 7. The d_{001} peak shifts to the left (lower angles) with respect to the peak of the pristine organoclay suggesting intercalation of the polymer molecules into the galleries of the clay.

WAXD data was analyzed using Bragg's Law which is defined as $n\lambda = 2d\sin\theta$, where n is an integer, λ is the wavelength of the X-ray beam incident on the object with lattice plane separation of d and θ is the Bragg angle. The 20A organoclay shows an intense peak at $2\theta = 3.8°$ which corresponds to a basal spacing of 23.2 Å. It can be seen that the compatibilizer system affects the organoclay interlayer spacing. The compatibilized

nanocomposites showed a modest shift to lower 2θ when compared to the nanocomposites without compatibilizer agent (Nano1), indicating some degree of polymer intercalation. Among the compatibilizer systems studied, the LLDPE-g-MA showed higher basal spacing ($2\theta = 2.7°$ which corresponds to a basal spacing of 33.0 Å); it suggests that the stacks of platelets are small when compared with the others compatibilizer systems. The intercalation and/or exfoliation process occurs preferentially in the amorphous phase. LLDPE-g-MA has a high melt index (and consequently low viscosity and crystallinity) which makes it an effective compatibilizer for this system. In addition to information about the type of structure formed in nanocomposites the X-ray scattering experiments were performed to
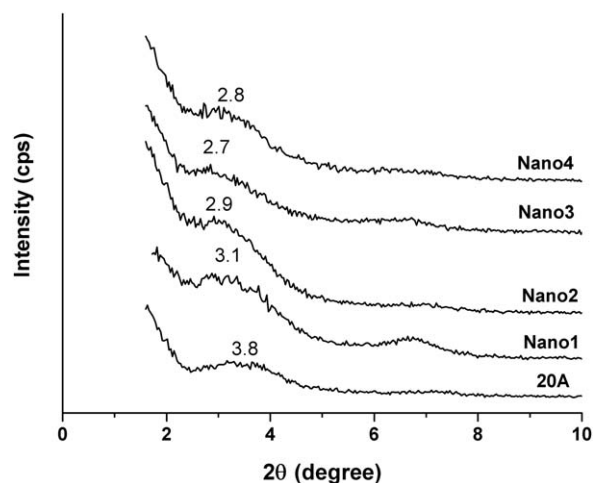

Figure 7. WAXD scans of pristine organoclay, 20A, and nanocomposites. The curves are vertically offset for clarity.
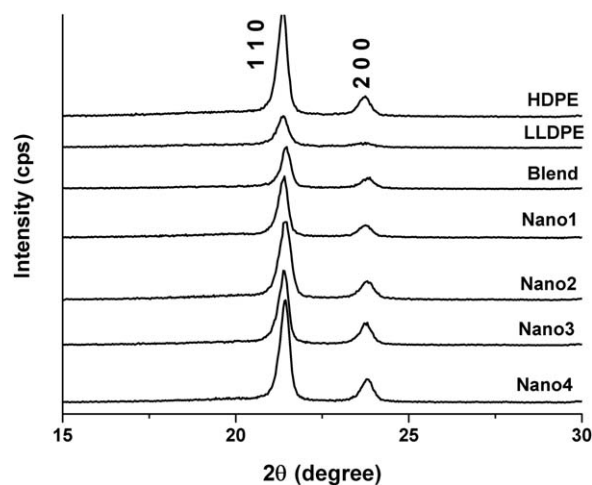
Figure 8. WAXD spectra in high angle region of HDPE, LLDPE, HDPE/LLDPE blend, and nanocomposites. The curves are vertically offset for clarity.

obtain information about the degree of crystallinity and crystallite size for the studied systems. The X-ray diffraction results are shown in Figure 8. It can be seen that all samples have two well-defined crystallographic planes (1 1 0) and (2 0 0). This clearly suggests that with addition of LLDPE, the characteristic orthorhombic structure of the crystals are retained, namely, the intrinsic crystal structure of HDPE has not been influenced.

DSC cooling scans, exhibiting the crystallization exotherm transitions, for HDPE, HDPE/LLDPE (75/25), and LLDPE samples are shown in Figure 9. The HDPE/LLDPE blend exhibited a single narrow exotherm (115°C). The higher crystallization temperature is perhaps conducive to forming HDPE-type crystallites in the blend. As no sign of two discrete exotherms or even peak broadening was observed, DSC results indicated that the two components in the blend (HDPE and LLDPE) were completely miscible at the molecular level and could co-crystallize.
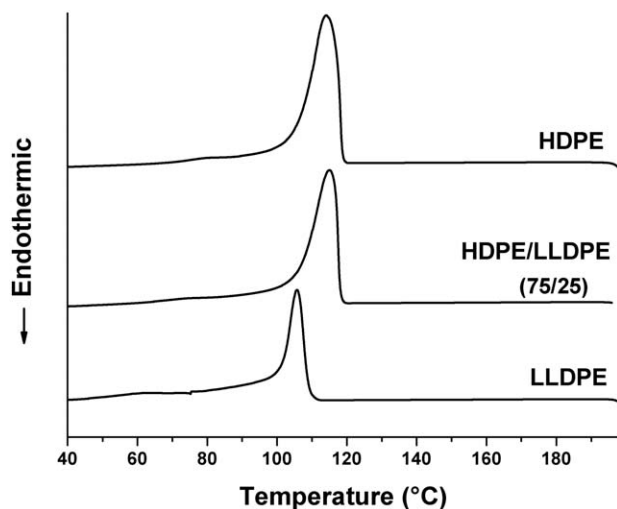
Figure 9. DSC cooling scans of HDPE, LLDPE, and HDPE/LLDPE blends. The curves are vertically offset for clarity.

Table IV. Values of Crystalline Parameters for HDPE, LLDPE, HDPE/LLDPE and Nanocomposites from X-Ray Data

Sample	Crystallinity (%)	Crystallite size (nm)
HDPE	72.9	52
LLDPE	54.1	38
Blend	63.1	48
Nano1	61.7	48
Nano2	61.9	41
Nano3	59.1	46
Nano4	64.2	49

The values of crystalline parameters for HDPE, LLDPE, HDPE/LLDPE, and nanocomposites are shown in Table IV. The degree of crystallinity is an important parameter for crystalline polymers and the determination of degree of crystallinity by X-ray diffraction has been claimed to be inherently superior to other methods. As it is known, the degree of crystallinity is dependent on the molecular structure of the polymer chains. The LLDPE molecules have higher content of short branched-chain segments that hinder its crystallization. Consequently, the degree of crystallinity of LLDPE is obviously smaller than that of HDPE. Also, the degree of crystallinity of the blend decrease proportionally to the addition of LLDPE. The similarity to the rate of crystallization of the HDPE indicates that the HDPE type of crystallization dominates in the blend. The faster growing crystallites of HDPE trapping nuclei of LLDPE, constituting HDPE like polyethylene segments in their growth process, could well explain the formation of HDPE type crystallites.[30,31] The composition of HDPE-type crystallites remain the same in the blend because that only linear chain segments participate in crystallization. Since the intercalation process occurs preferentially in the amorphous phase and the LLDPE-g-MA has a lower crystallinity than the HDPE-g-MA, the compatibilizer systems with LLDPE-g-MA (Nano3) or mixture of compatibilizers (Nano4) showed greater intercalation of the HDPE/LLDPE nanocomposites compared to compatibilizer system with HDPE-g-MA (Nano2).

The apparent crystallite size was calculated in the (110) plane that correspond to the diagonal plane a–b. Concerning the intermolecular heterogeneity between HDPE and LLDPE (for instance, the difference in a average molecular weight), in the rich domain of one macromolecule, the regular arrangement of the chain segments of the other species might be excluded during crystallization, accordingly the original crystalline thermodynamics state of the given macromolecule is altered.[34] As a result, the crystal size becomes smaller.

Rheological Characterization of the Nanocomposites
Figure 10 shows the $\eta(\dot{\gamma})$ curves of HDPE, LLDPE, HDPE/LLDPE blend, and the nanocomposites obtained from different compatibilizer systems.

The LLDPE shows predominantly Newtonian behavior while the HDPE has a Newtonian plateau and a power-law behavior with the increase of shear rate. The HDPE/LLDPE blend also has a short Newtonian plateau at low shear rates. The steady-
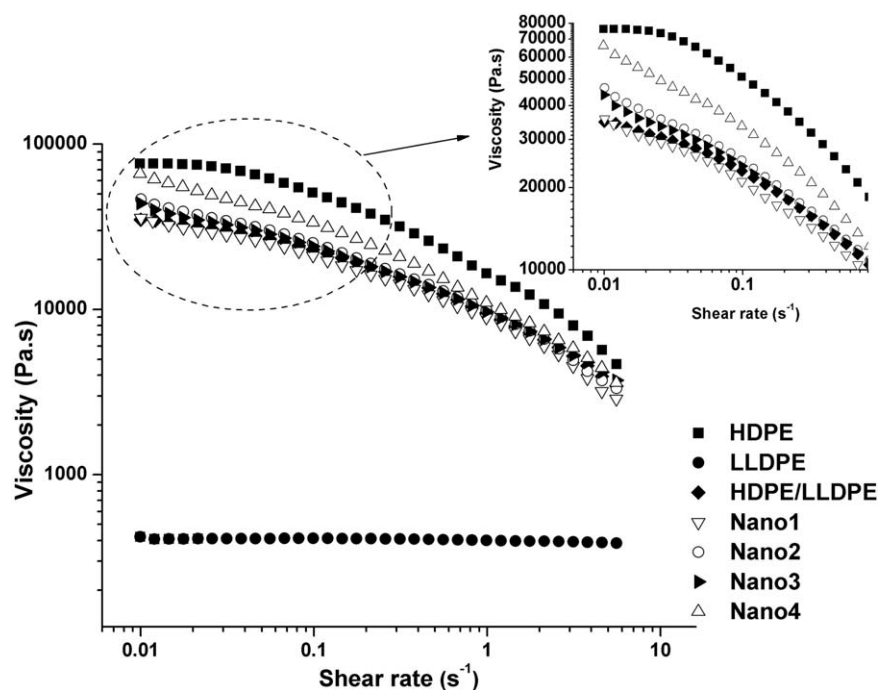
Figure 10. Steady-state shear viscosity of HDPE, LLDPE, HDPE/LLDPE blend, and nanocomposites at 180°C.

state rheological properties showed that the addition of organoclay to the HDPE/LLDPE increased the shear viscosity at low shear rates, changing the behavior of HDPE/LLDPE matrix to a more pronounced shear thinning one. In nanocomposites materials with highly interpenetrated or connected structures, the Bingham model behavior can be observed. The slope of the log η versus log $\dot{\gamma}$ curve has been used to describe the structure of nanocomposites since when m → 0 the viscosity tends to a constant value (Newtonian, viscous liquid), whereas when m → −∞ the behavior observed is similar to that of an elastic solid (the curve slope tends to −1 and the material presents a Bingham model behavior).[6,35,36]

The nanocomposites compatibilized with LLDPE-*g*-MA (Nano 3) and mixture of HDPE-*g*-MA/LLDPE-*g*-MA (Nano 4) showed similar slopes (−0.49 and −0.47, respectively). The Nano 2 had the high slope (−0.42) among the compatibilizer systems studied. This result can be an indicative that the interactions between the matrix and the nanoclay are stronger in LLDPE-*g*-MA-compatibilized system and mixture of HDPE-*g*-MA/LLDPE-*g*-MA than in HDPE-*g*-MA-compatibilized system; therefore, it also indicates that Nano 3 has better nanoclay's distribution than Nano 2.

TEM Analysis

TEM micrographs of HDPE/LLDPE blend-based nanocomposites provide a direct visualization of the degree of organoclay intercalation or exfoliation in these materials. Figure 11 shows the TEM micrographs of the nanocomposites. The Nano1 shows several aggregates, formed by large tactoids poorly dispersed in the HDPE/LLDPE matrix, as is clearly seen in Figure 11(a). This TEM image correlates with WAXD and rheological analysis, which indicated weak interactions between the matrix and

nanoclay and poor dispersion for the nanocomposite without addition of compatibilizer agent.

The TEM micrographs for Nano2, Nano3, and Nano4 show an intercalated morphology with a small number of individual platelets dispersed in the HDPE/LLDPE matrix plus some small tactoids. With regard to compatibilized nanocomposites, TEM images are also in agreement with WAXD and rheology. The compatibilizer's addition in the polymer matrix improved the intercalation of the nanoclays due to presence of polar MA groups. The LLDPE-*g*-MA has a lower viscosity which facilitated the dispersion of Cloisite 20A and, consequently, improved the interactions between matrix and organoclay.
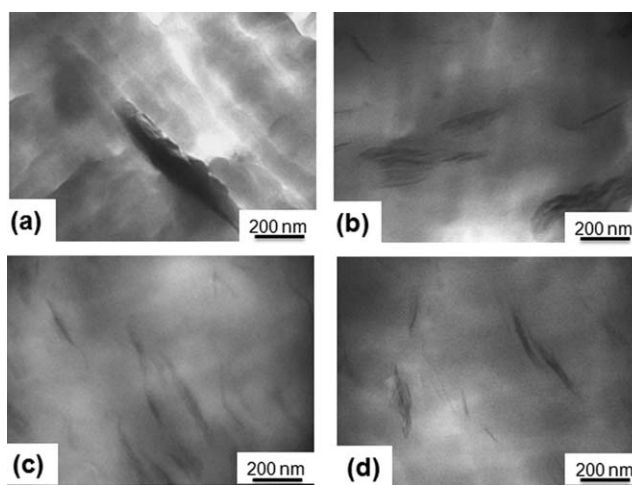

Figure 11. TEM micrographs of nanocomposites: (a) Nano1; (b) Nano2; (c) Nano3, and (d) Nano4 (88,000×).
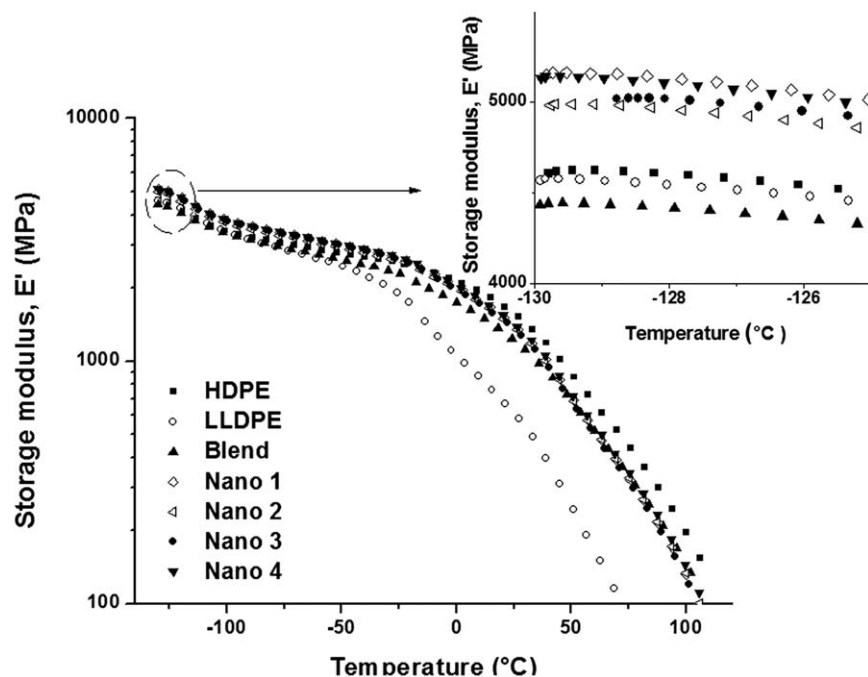
Figure 12. Storage modulus of HDPE, LLDPE, HDPE/LLDPE blend, and the nanocomposites as a function of temperature.

DMA Analysis

The temperature dependence of the storage modulus (E') of the HDPE, LLDPE, blend, and nanocomposites was also investigated. Figure 12 shows the DMA curves of the samples.

The presence of organoclay in HDPE/LLDPE blend causes an increase in the storage modulus, while the presence of relatively soft compatibilizer causes a decrease of the storage modulus due to effect of maleation on crystallinity or crystalline structure. Thus, the storage modulus of compatibilized nanocomposites was lower than that of nanocomposites without compatibilizer agent (Nano1). Interestingly, there seems to be no advantage in adding compatibilizer agent for building storage modulus at low organoclay content (2.5%) since the curves for non-compatibilized system (Nano1) and compatibilized systems (Nano2, Nano3, and Nano4) are virtually the same in this region, in spite of the morphological differences seen. Spencer[19] and Hotta[24] showed that the mechanical performance of the system is not only governed by the clay exfoliation and clay content but also by the presence of a significant amount of the compatibilizer agent. On the other hand, in the absence of compatibilizer agent, the modulus decreases with the addition of organoclay beyond about 2.5%.

Thus, there is a clear advantage of adding maleic anhydride grafted polyethylene in the nanocomposites that is not only promoting the exfoliation and/or intercalation of the clays but also improving adhesion of the organoclay to the HDPE/LLDPE blend. It can be seen for the compatibilizer systems studied that LLDPE-g-MA (Nano3) and mixture of LLDPE-g-MA and HDPE-g-MA increase the storage modulus when compared to systems with only HDPE-g-MA (Nano2) as compatibilizer. This difference observed suggests that LLDPE-g-MA may promote adhesion to the clay particles.

CONCLUSIONS

In this study, HDPE/LLDPE blend-based nanocomposites were prepared by melt processing using three different compatibilizer systems (LLDPE-g-MA, HDPE-g-MA, and 50/50 wt % mixture of these compatibilizers). Structural properties and thermal mechanical performance were investigated by several characterization techniques. It was observed that during the preparation of the MB crosslinking formation between the polyethylene chains occurred and this fact could be correlated to the mechanisms involved in the polyethylene degradation. The small amounts of crosslinking do not interfere in the nanocomposites processing. A schematic representation of the increase in the interlayer distance with the diffusion of the crosslinked polyethylene was proposed.

The compatibilizer system affects the organoclay interlayer spacing. Among the compatibilizer systems studied, the LLDPE-g-MA showed higher basal spacing suggesting that the stacks of platelets are small when compared with the others compatibilizer systems. LLDPE-g-MA has a lower viscosity and facilitated the dispersion of 20A and, consequently, improved the interactions between matrix and organoclay which makes it an effective compatibilizer for this system. The steady-state rheological properties showed that the nanoclay's addition to the HDPE/LLDPE increased the shear viscosity at low shear rates, changing the behavior of HDPE/LLDPE matrix to a more pronounced shear thinning one. Compatibilized nanocomposites exhibited an intercalated morphology with a small number of individual platelets dispersed in the HDPE/LLDPE matrix and the mechanical performance of the system is not governed only by the clay exfoliation and clay content but also by the presence of a significant amount of the compatibilizer agent.

ACKNOWLEDGMENTS

REFERENCES

1. Liu, C.; Wang, J.; He, J. *Polymer* **2002**, *43*, 3811.

2. Choi, P. *Polymer* **2000**, *41*, 8741.

3. Quental, A. C.; Felisberti, M. I. *Eur. Polym. J.* **2005**, *41*, 894.

4. Munaro, M.; Akcelrud, L. *Polym. Degrad. Stab.* **2008**, *93*, 43.

5. Hussein, I. A. *Macromolecules* **2003**, *36*, 2024.

6. Teymouri, Y.; Nazockdast, H. *J. Mater. Sci.* **2011**, *20*, 6642.

7. Xu, J. T.; Zhao, Y. Q.; Wang, Q.; Fan, Z. Q. *Polymer* **2005**, *46*, 11978.

8. Zanetti, M.; Costa, L. *Polymer* **2004**, *45*, 4367.

9. Passador, F. R.; Ruvolo-Filho, A. C.; Pessan, L. A. *Polímeros* **2012**, *22*, 357.

10. Durmus, A.; Kasgoz, A.; Macosko, C. W. *Polymer* **2007**, *48*, 4492.

11. Ishida, H.; Campbell, S.; Blackwell, J. *Chem. Mater.* **2000**, *12*, 1260.

12. Durmus, A.; Woo, M.; Kasgoz, A.; Macosko, C. W.; Tsapatsis, M. *Eur. Polym. J.* **2007**, *43*, 3737.

13. Fornes, T. D.; Yoon, P. J.; Keskkula, H.; Paul, D. R. *Polymer* **2001**, *42*, 9929.

14. Alexandre, M.; Dubois, P. *Mater. Sci. Eng.* **2000**, *28*, 1.

15. Kato, M.; Okamoto, N.; Hasegawa, A.; Tsukigase, A.; Usuki, A. *Polym. Eng. Sci.* **2003**, *43*, 1312.

16. Martins, C. G.; Larocca, N. M.; Paul, D. R.; Pessan, L. A. *Polymer* **2009**, *50*, 1743.

17. Marini, J.; Branciforti, M. C.; Alves, R. M. V.; Bretas, R. E. S. *J. Appl. Polym. Sci.* **2010**, *118*, 3340.

18. Chinellato, A. C.; Vidotti, S. E.; Hu, G.-H.; Pessan, L. A. *Compos. Sci. Tech.* **2010**, *70*, 458.

19. Spencer, M. W.; Cui, L.; Yoo, Y.; Paul, D. R. *Polymer* **2010**, *51*, 1056.

20. Wang, K. H.; Choi, M. H.; Koo, C. M.; Choi, Y. S.; Chung, I. *J. Polymer* **2001**, *42*, 9819.

21. Picard, E.; Vermogen, A.; Gérard, J-F.; Espuche, E. *J. Polym. Sci. Part B Polym. Phys.* **2008**, *46*, 2593.

22. Chrissopoulou, K.; Altintzi, I.; Anastasiadis, S. H.; Giannelis, E. P.; Pitsikalis, M.; Hadjichristidis, N.; Theophilou, N. *Polymer* **2005**, *46*, 12440.

23. Morawiec, J.; Pawlak, A.; Slouf, M.; Galeski, A.; Piorkowska, E.; Krasnikowa, N. *Eur. Polym. J.* **2005**, *41*, 1115.

24. Hotta, S.; Paul, D. R. *Polymer* **2004**, *45*, 7639.

25. Gopakumar, T. G.; Lee, J. A.; Kontopoulou, M.; Parent, J. S. *Polymer* **2002**, *43*, 5483.

26. Ryu, S. H.; Chang, Y. W. *Polym. Bull.* **2005**, *55*, 385.

27. Gonzáles-Montiel, A.; Keskkula, H.; Paul, D. R. *J. Polym. Sci. Part B: Polym. Phys.* **1995**, *33*, 1751.

28. Huang, J. J.; Keskkula, H.; Paul, D. R. *Polymer* **2006**, *47*, 624.

29. Shah, R. K.; Kim, D. H.; Paul, D. R. *Polymer* **2007**, *48*, 1047.

30. Dintcheva, N. Tz.; Al-Malaika, S.; La Mantia, F. P. *Polym. Degrad. Stab.* **2009**, *94*, 1571.

31. Mainil, M.; Alexandre, M.; Monteverde, F.; Dubois, P. *J. Nanosci. Nanotechnol.* **2006**, *6*, 337.

32. Pages, P.; Carrasco, F.; Saurina, J.; Colom, X. *J. Appl. Polym. Sci.* **1996**, *60*, 153.

33. Carrasco, F.; Pages, P.; Pascual, S.; Colom, X. *Eur. Polym. J.* **2001**, *37*, 1457.

34. Rana, S. K. *J. Appl. Polym. Sci.* **2002**, *83*, 2604.

35. Wagener, R.; Reisinger, T. J. G. *Polymer* **2003**, *44*, 7513.

36. Lotti, C.; Isaac, C. S.; Branciforti, M. C.; Alves, R. M. V. Liberman, S.; Bretas, R. E. S. *Eur. Polym. J.* **2008**, *44*, 1346.